JOURNAL OF MATERIALS SCIENCE LETTERS 12 (1993) 1774–1777

Rapid eutectic growth of undercooled metallic alloys

B. WEI*, D. M. HERLACH
Institut für Raumsimulation, Deutsche Forschungsanstalt für Luftund Raumfahrt, D-5000 Köln 90, Germany

F. SOMMER
Max-Planck-Institut für Metallforschung, D-7000 Stuttgart 1, Germany

Both growth velocity and interlamellar spacing were measured as functions of the undercooling of a eutectic $Co_{74.5}Sb_{25.5}$ alloy. A lamellar eutectic/anomalous eutectic growth-morphology transition was observed. Two critical undercooling thresholds were determined: below the lower limit of $\Delta T^*_{e1} = 50$ K, lamellar growth is the unique growth morphology; above the upper limit of $\Delta T^*_{e2} = 150$ K, only an anomalous eutectic can grow. Although this is qualitatively compatible with the prediction of the modern theory of eutectic growth that a maximum-growth-velocity limit exists for coupled lamellar eutectic growth, the formation of an anomalous eutectic discredits the applicability of the current physical models for eutectic growth to rapid solidication.

Crystal-growth phenomena in undercooled melts have been the subject of intense research. In particular, dendritic growth has been studied both from a theoretical [1–3] and an experimental viewpoint [4–6]. Dendritic growth is a single-phase-growth mechanism and has been comparatively well solved.

Eutectic growth involves the interacting nucleation and co-operative growth of two or more solid phases within one liquid phase. Since the pioneering work by Jackson and Hunt (JH) [7], eutectic growth has attracted extensive attention [8–11].

Assuming that the interlamellar spacing, λ, is much smaller than the diffusion distance, D_L/V (where D_L and V are the solute diffusion coefficient in liquid and the eutectic growth velocity, respectively), and that the interface undercooling is sufficiently small so that the interface composition is approximately the same as the eutectic concentration, JH derived the well-known relationship between the undercooling, ΔT, the growth velocity, V, and the interlamellar spacing, λ:

$$\Delta T = K_1 V\lambda + K_2/\lambda \quad (1)$$

where K_1 and K_2 are constants depending only on the alloy system. By further postulating that the eutectic grows under an extremum condition, which was subsequently justified by stability analysis [8–10], they arrived at the final conclusions

$$\lambda^2 V = K_2/K_1 = \text{constant} \quad (2a)$$

$$\lambda\Delta T = 2K_2 = \text{constant} \quad (2b)$$

$$\Delta T^2 V = 4K_1K_2 = \text{constant} \quad (2c)$$

These have proven to be the most successful physical model for regular lamellar (or rod) eutectic growth during the usually slow solidification process where the Peclet number, $P_e = V\lambda/2D_L$ is smaller than unity.

However, rapid solidification processing has thrown up a challenge for the JH eutectic-growth theory in two categories of experimental achievements. First, the solidification velocity can exceed 1 m s^{-1} when a laser or an electron beam is used for surface melting and resolidification. In such a case, the diffusion distance becomes small and the undercooling is very large so that the two assumptions used by JH must be relaxed. Furthermore, a maximum growth-velocity limit has been observed for Al–Cu [12] and Ag–Cu [13] eutectic alloys; beyond this limit, coupled lamellar growth can no longer occur. Secondly, a growth-morphology transition from regular lamellar eutectic to anomalous eutectic takes place during the rapid solidification of some bulk undercooled binary eutectics [14–19], if the undercooling is sufficiently large. This indicates that the JH theory is applicable only below a certain critical undercooling where regular lamellar eutectic growth is ensured.

In an effort to explain the limiting velocity for co-operative growth, Trivedi, Magnin and Kurz (TMK) [20] extended the JH analysis to rapid-solidification conditions. According to the TMK model, the JH theory shows significant deviations from the actual growth condition when the Peclet number exceeds unity. This model reveals that the origin of the eutectic-growth limit is either the temperature dependence of the diffusion coefficient or the limit of undercooling. Recently, Kurz and Trivedi [21] have developed a more complete form for their new model which includes nonequilibrium effects, in particular, interface solute trapping. In brief, the TMK theory predicts that the right-hand sides of Equation 2 are not constants:

$$\lambda^2 V = f_1(V, P_e) \quad (3a)$$

$$\lambda\Delta T = f_2(V, P_e) \quad (3b)$$

$$\Delta T^2/V = f_3(V, P_e) \quad (3c)$$

where f_1, f_2 and f_3 are functions of the eutectic-growth velocity and the Peclet number. So far, there have been no experimental investigations of eutectic

*On leave from the Northwestern Polytechnical University, People's Republic of China.

0261-8028

growth in undercooled alloy melts. However, quantitative measurements of the eutectic-growth velocity, as a function of undercooling, are necessary before a significant analysis of rapid anomalous eutectic growth can be made. This letter reports experimental measurements of both the growth velocity and the interlamellar spacing over extended levels of undercooling. The results allow for a clear distinction between the undercooling regime where current theories of eutectic growth are applicable and those where these physical models become invalid. In particular, the critical undercoolings have been determined at which the predictions of eutectic-growth theories failed.

The experiments were accomplished with a glass-flux undercooling facility [22] under an 80 kPa He–20% H_2 atmosphere. An *in situ* alloying procedure was used to prepare $Co_{74.5}Sb_{25.5}$ alloy samples, during an experiment, from 99.998% pure Co and 99.9999% pure Sb by radio-frequency (r.f.) induction melting. Each sample had a mass of 1 g and was immersed within a pool of molten boron-silicate glass in an 8 mm inner diameter by 10 mm outer diameter by 15 mm alumina crucible. The samples' undercoolings were measured with a two-colour infrared pyrometer at an accuracy of about ±3 K. The recalescence time during solidification was measured by a specially designed infrared photodiode device, which consisted of a quartz lens and a S153P photodiode (with a sensitive area of 2.8 mm × 2.8 mm and a response time of 50 ns). This device was so constructed and installed that the whole image of the sample was focused onto the sensitive area of the photodiode. Both the pyrometer and the photodiode device were coupled to a WTW/SMR-2 transient-signal memory recorder, which displayed the sampling rate up to 10 MHz. The sample mass assured that the display took the shape of a pancake, whose thickness was much smaller than its diameter, during solidification. This, together with visual observations of the recalescence event, made this a convenient procedure to judge whether nucleation occurred on the upper surface of sample, which proved to be the side preferable for nucleation. Because the recalescence front was a sharply visible interface between hotter and colder parts of the sample, which swept across the sample surface, the recalescence velocity was taken to a first-order approximation as the ratio of the sample size to the recalescence time. Under such a definition, the measured recalescence velocity showed rather large scatter, since nucleation could take place simultaneously at more than one site. The actual recalescence velocity should be the lower limit of all the different data obtained for a certain undercooling, which corresponds to the situation of a single nucleation event at the periphery of the sample surface. This means that a large number of experiments were necessary to get the true physical information. A total of 45 independent experiments were made, with each sample being melted and solidified several times. After an experiment, the eutectic microstructures were analysed following usual metallographic procedures. Because the movement of the recalescence interface was driven by the advancing solid–liquid interface, or the eutectic-growth front, the measured recalescence velocity provided information about the eutectic-growth velocity.

As shown in Fig. 1, the eutectic-growth morphology of $Co_{74.5}Sb_{25.5}$ alloy transformed from a regular lamellar eutectic to a kind of anomalous eutectic as undercooling increased. Below a lower undercooling limit of about $\Delta T_{e1}^{*} = 50$ K, regular lamellar eutectic was the unique microstructure. Above an upper

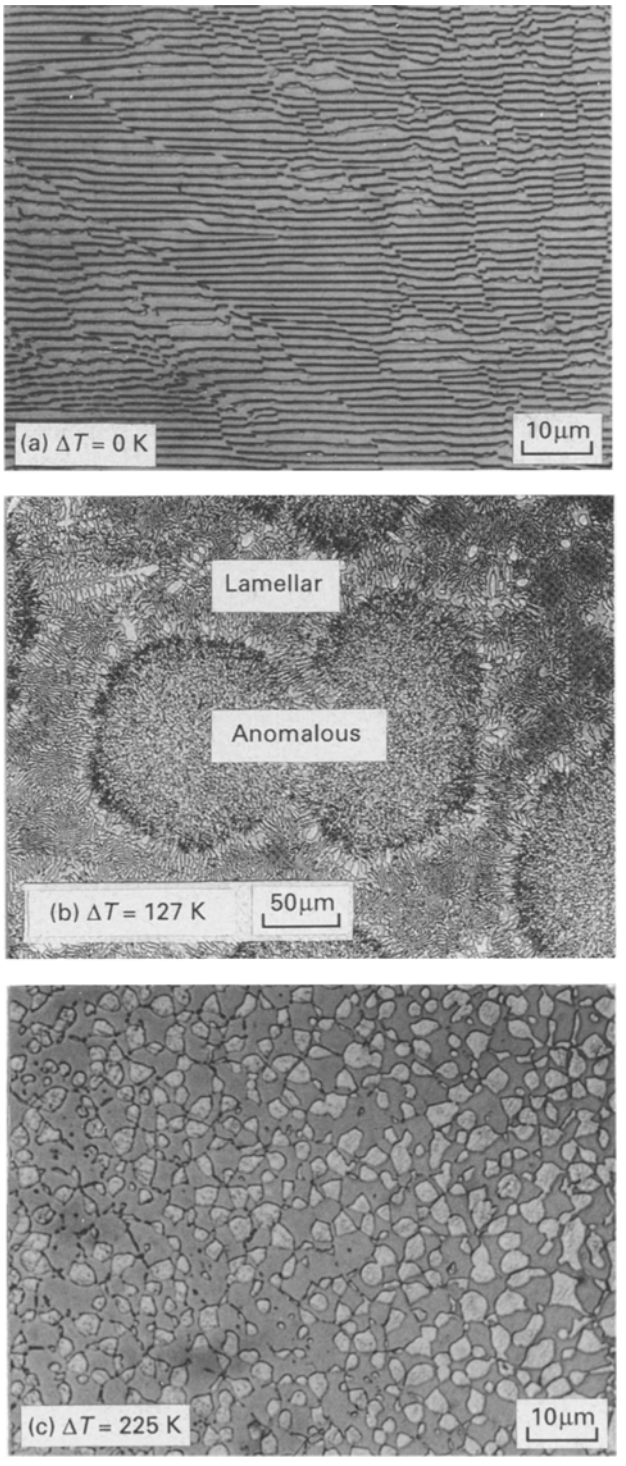

Figure 1 Eutectic-growth morphologies at different undercoolings: (a) lamellar eutectic ($\Delta T = 0$ K), (b) mixed eutectic microstructures consisting of lamellar and anomalous eutectics ($\Delta T = 127$ K), and (c) anomalous eutectic ($\Delta T = 225$ K).

threshold $\Delta T^*_{e2} = 150$ K, anomalous eutectic replaced lamellar eutectic completely. In the intermediate undercooling range, both kinds of eutectic structures coexisted with the volume fraction of anomalous eutectic increasing with undercooling. Within the sample undercooled by 127 K, whose solidification microstructure is shown in Fig. 1b, anomalous eutectic occupied approximately 90% of the volume. Macroscopically, a lot of anomalous-eutectic grains with a diameter ranging from 0.08 to 1.7 mm are distributed rather homogeneously in the sample. The intergranular spaces are filled with lamellar eutectics, most of which have grown epitaxially from the growth front of rapid solidification, whereas lamellar eutectic forms under slow-solidification conditions.

Fig. 2 presents the measured average interlamellar spacing versus undercooling with a comparison of the results calculated from the JH and TMK eutectic-growth models. In order to apply the TMK model, the α-Co and β-CoSb phases are assumed to show equal solute partition coefficients, which is compatible with the characteristics of a Co–Sb phase diagram [23]. The physical parameters used for the calculations are listed in Table I. It is interesting that the difference between the calculated interlamellar spacings of JH and TMK models is negligibly small. When undercooling is below the lower threshold of ΔT^*_{e1}, the experimental data agree fairly well with the calculations. However, the spacings of intergranular lamellar eutectic remain almost independent of the undercooling and tend to maintain the interlamellar spacing of extremely small undercooling, once the undercooling exceeds ΔT^*_{e1}, so that anomalous eutectic appears. This is because anomalous eutectic forms during recalescence if the alloy melt is undercooled to the intermediate range between ΔT^*_{e1} and ΔT^*_{e2}. Since the remnant undercooling after recalescence is considerably lower, lamellar eutectic grows slowly within the intergranular spaces between adjacent anomalous grains, resulting in lamellar spacings comparable to the case of negligible undercooling.

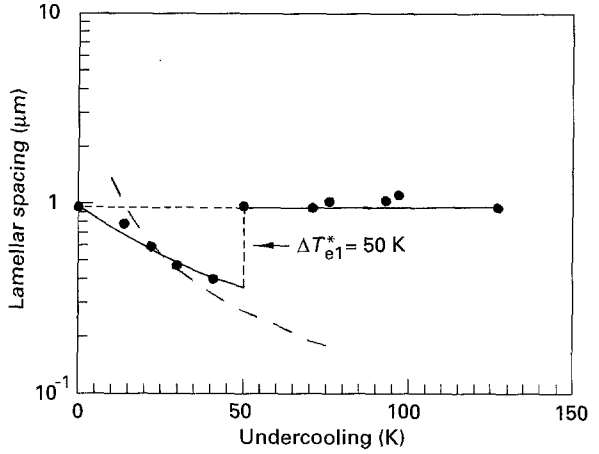

Figure 2 Interlamellar spacings as a function of undercooling: (●) experimental data and (---) JH and TMK models. The results calculated from the JH and TMK models are negligibly different.

TABLE I Material parameters used for calculations of the eutectic solidification of Co–Sb with $A = 3.32 \times 10^{-7}$ and $B = 55618$

Parameter	Unit	Value
C_e	Atomic fraction	0.255
T_e	K	1368
f_α	Volume fraction	0.356
f_β	Volume fraction	0.654
m_α	K(fraction)$^{-1}$	1569
m_β	K(atomic fraction)$^{-1}$	476
k_α, k_β	Dimensionless	0.2
a_L	m(atomic fraction)	1.86×10^{-8}
D_L	m^2 s^{-1}	$A \exp - B/RT$
V_d	m s^{-1}	19

Fig. 3 shows the measured recalescence velocities and calculated eutectic-growth velocities at different undercooling levels. It should be noted that the calculations from the JH and TMK only make sense for lamellar eutectic. When undercooling exceeds ΔT^*_{e1}, the experimental data correspond to anomalous-eutectic growth. Because of the intrinsically approximate nature of the present measurements, the lower limits of the experimental results should coincide with the actual recalescence velocities, which can be best fitted by a power relation of 12.9 $(\Delta T - 37)^{0.62}$ mm s^{-1}. When only lamellar or anomalous eutectic grows, the recalescence velocity serves as an upper limit to the actual eutectic-growth velocity. In the intermediate undercooling regime where both anomalous and lamellar eutectics form, a better approximation of the anomalous-eutectic-growth velocity is the ratio of anomalous-eutectic grain size to recalescence time, which is shown by the asterisks in Fig. 3. It is clear that the recalescence velocity is quite different from the anomalous eutectic-growth velocity in this range. Evidently, both the JH and the TMK models are in agreement with experiment when lamellar eutectic is ensured to be the unique growth morphology below ΔT^*_{e1}.

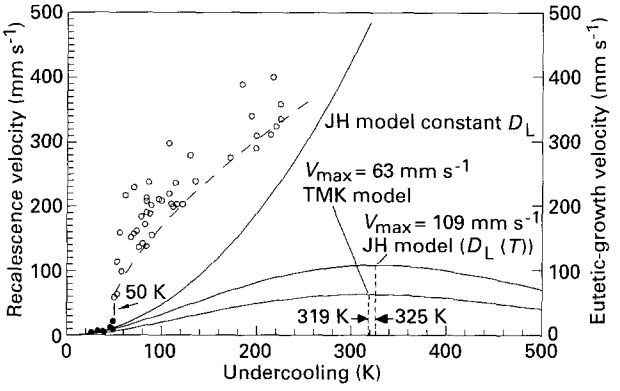

Figure 3 Measured recalescence velocity and calculated eutectic-growth velocity as a function of undercooling. (●) Measured recalescence velocity for lamellar eutectic growth; (○) measured recalescence velocity for anomalous-eutectic growth; (---) best fitting for the predicted actual recalescence velocity of anomalous-eutectic growth; (*) a better approximation for the anomalous-eutectic-growth velocity in the intermediate undercooling regime, which is the ratio of an anomalous-eutectic grain size to recalescence time; and (—) calculated eutectic-growth velocities of the JH model (with a constant solute-diffusion coefficient, D_L and a temperature dependent D_L) and the TMK model (with a temperature dependent D_L, taking into account the non-equilibrium interface kinetic effect).

Nevertheless, the growth velocity of anomalous eutectic varies with the undercooling in a manner quite different from these lamellar-eutectic-growth models. In fact, the anomalous-eutectic-growth velocity is significantly larger then the lamellar-eutectic-growth velocities calculated from the TMK model. The main feature of the TMK model is that it predicts a maximum-growth-velocity limit of 63 mm s^{-1} for the $Co_{74.5}Sb_{25.5}$ lamellar eutectic at an undercooling of 319 K. In contrast, the experimentally observed maximum recalescence velocity induced by lamellar eutectic growth is only 22 mm s^{-1}, which corresponds to an undercooling slightly below ΔT^*_{e1}. If a constant solute-diffusion coefficient, D_L, is assumed, the JH model gives a parabolic relation for the eutectic-growth velocity as a function of the undercooling as determined by Equation 2, and no growth-velocity limit is expected. However, when the temperature dependence of the diffusion coefficient is taken into consideration, the JH model also exhibits a maximum lamellar-eutectic-growth velocity of 109 mm s^{-1} at a 325 K undercooling. Although the maximum growth velocities predicted by the JH and the TMK models are quite different, the corresponding undercoolings are close to each other. This means that in the case of $Co_{74.5}Sb_{25.5}$ lamellar eutectic growth the limiting growth velocity results from the temperature-dependent solute diffusion.

Although the fact that two undercooling thresholds exist for the eutectic-growth-morphology transition is compatible with the prediction of a lamellar-eutectic-growth velocity limit by the TMK model, there is a significant difference between rapid solidification of bulk undercooled alloy melts and laser or electron-beam surface treatment. That is, the latter processing is characterized by rapid epitaxial growth and it usually does not involve nucleation. In contrast, crystal nucleation plays as important a role as growth kinetics during rapid eutectic growth in undercooled melts. This explains why the banded structures produced by surface resolidification beyond the lamellar-eutectic-growth-velocity limit [12, 13] are essentially different from the anomalous eutectics of the same alloys [14, 15]. On the other hand rapid quenching usually results in similar anomalous-eutectic structures [24, 25], because this is actually a transient undercooling process.

To sum up, a lamellar eutectic/anomalous eutectic growth morphology transition was observed during the rapid solidification of a $Co_{74.5}Sb_{25.5}$ eutectic alloy which was undercooled by up to 225 K. Two undercooling thresholds were determined experimentally: below the lower limit of $\Delta T^*_{e1} = 50$ K, regular lamellar eutectic is the unique growth morphology; above the upper limit of $\Delta T^*_{e2} = 150$ K, only anomalous eutectic can grow. This is in qualitative agreement with the prediction of the TMK-eutectic-growth model that a maximum growth-velocity limit exists beyond which coupled lamellar eutectic growth is impossible. Experimental results indicate that the maximum growth velocity of a $Co_{74.5}Sb_{25.5}$ lamellar eutectic is about 22 mm s^{-1} in an undercooled melt. The growth velocity of anomalous eutectic is much higher than the prediction of the TMK model for lamellar eutectic growth, and it assumes a quite different undercooling dependence. Both the JH and the TMK models are aimed at regular lamellar eutectic growth and hence they become invalid once an anomalous eutectic appears.

Acknowledgement

The authors thank B. Feuerbacher for continuous support and W. Kurz for helpful discussions. B. Wei is grateful to Alexander von Humboldt Stiftung for the financial support which made this work possible. He is also indebted to G. P. Görler, D. Holland-Moritz, S. Sauerland, M. Barth and T. Volkmann for their consistent help.

References

1. R. C. BROWER, D. A. KESSLER, J. KOPLIK and H. LEVINE, *Phys. Rev. Lett.* **51** (1983) 1111.
2. E. BEN-JACOB N. GOLDENFELD, J. S. LANGER and G. SCHÖN, *ibid.* **51** (1983) 1930.
3. D. A. KESSLER and H. LEVINE, *ibid.* **57** (1986) 3069.
4. A. DOUGHERTY, P. D. KAPLAN and J. P. GOLLUB, *ibid.* **58** (1987) 1652.
5. H. CHOU and H. Z. CUMMINS, *ibid.* **61** (1988) 173.
6. R. WILLNECKER, D. M. HERLACH and B. FEUERBACHER, *ibid.* **62** (1989) 2709.
7. K. A. JACKSON and J. D. HUNT, *Trans Met. Soc. AIME* **236** (1966) 1129.
8. J. S. LANGER, *Phys. Rev. Lett.* **44** (1980) 1023.
9. V. DATYE and J. S. LANGER, *Phys. Rev. B* **24** (1981) 4155.
10. S. STRÄSSLER and W. R. SCHNEIDER, *Phys. Cond. Matter* **17** (1974) 153.
11. A. KARMA and A. SARKISSIAN, *Phys. Rev. Lett.* **68** (1992) 2616.
12. M. ZIMMERMANN, M. CARRARD and W. KURZ, *Acta Metall.* **37** (1989) 3305.
13. W. J. BOETTINGER, D. SHECTMAN, R. J. SCHAEFER and F. S. BIANCANIELLA, *Metall Trans. A* **15** (1971) 55.
14. B. L. JONES, *ibid.* **2** (1971) 1950.
15. B. L. JONES, G. M. WESTON and R. T. SOUTHIN, *J. Cryst. Growth* **10** (1971) 313.
16. M. G. CHU, Y. SHIOHARA and M. C. FLEMINGS, *Metall. Trans. A* **15** (1984) 1303.
17. B. WEI, G. YANY and Y. ZHOU, *Acta Metall. Mater. A* **15** (1991) 1303.
18. Y. R. S. MURTY and T. Z. KATTAMIS, *J. Cryst. Growth* **22** (1974) 219.
19. S. N. TEWARI, *Metall. Trans. A* **18** (1987) 525.
20. R. TRIVEDI, P. MAGNIN and W. KURZ, *Acta Metall.* **35** (1987) 971.
21. W. KURZ and R. TRIVEDI, *Metall. Trans. A* **22** (1991) 3051.
22. E. SCHLEIP, D. M. HERLACH and B. FEUERBACHER, *Europhys. Lett.* **11** (1990) 751.
23. T. B. MASSALSKI, "Binary alloy phase diagrams", Vol. 1 (American Society for Metals, Metals Park, Ohio, 1986) p. 798.
24. R. CHEESE and B. CANTOR, *Mater. Sci. Engng* **45** (1980) 83.
25. D. B. WILLIAMS and J. W. EDINGTON, *J. Mater. Sci.* **12** (1977) 126.

Received 7 January
and accepted 20 May 1993